

El Niño-Southern Oscillation Complexity

Axel Timmermann^{1,2}, Soon-Il An³, Jong-Seong Kug⁴, Fei-Fei Jin⁵, Wenju Cai⁶, Antonietta Capotondi^{7,8}, Kim Cobb⁹, Matthieu Lengaigne¹⁰, Michael J. McPhaden¹¹, Malte F. Stuecker^{12,13}, Karl Stein¹, Andrew T. Wittenberg¹⁴, Kyung-Sook Yun¹, Tobias Bayr¹⁵, Han-Ching Chen¹⁶, Yoshimitsu Chikamoto¹⁷, Boris Dewitte¹⁸, Dietmar Dommenget¹⁹, Pamela Grothe²⁰, Eric Guilyardi^{21,22}, Yoo-Geun Ham²³, Michiya Hayashi⁵, Sarah Ineson²⁴, Daehyun Kang²⁵, Sunyong Kim⁴, WonMoo Kim²⁶, June-Yi Lee¹, Tim Li^{2,5}, Jing-Jia Luo²⁷, Shayne McGregor¹⁹, Yann Planton²¹, Scott Power²⁷, Harun Rashid⁶, Hong-Li Ren²⁸, Agus Santoso²⁹, Ken Takahashi³⁰, Alexander Todd³¹, Guomin Wang²⁷, Guojian Wang⁶, Ruihuang Xie³², Woo-Hyun Yang⁴, Sang-Wook Yeh³³, Jinho Yoon³⁴, Elke Zeller¹, Xuebin Zhang³⁵

¹Center for Climate Physics, Institute for Basic Science (IBS), Pusan National University, Busan, Republic of Korea

²International Pacific Research Center, University of Hawaii at Manoa, Honolulu, Hawaii, USA.

³Department of Atmospheric Sciences, Yonsei University, Seoul, Korea

⁴Division of Environmental Science & Engineering, Pohang University of Science and Technology (POSTECH), Pohang 37673, South Korea

⁵Department of Atmospheric Science, SOEST, University of Hawaii at Manoa, Honolulu, Hawaii, USA

⁶CSIRO Oceans and Atmosphere, Aspendale, Victoria 3195, Australia

⁷Cooperative Institute for Research in Environmental Science, University of Colorado, Boulder CO, 80309, USA

⁸Physical Sciences Division, NOAA Earth System Research Laboratory, Boulder CO, 80305, USA

⁹Earth & Atmospheric Sciences, Georgia Tech, MC 0340 311 Ferst Drive Atlanta, USA

¹⁰Sorbonne Universités (UPMC, Univ. Paris 06) CNRS-IRD-MNHN, LOCEAN laboratory, IPSL, Paris, France

¹¹Pacific Marine Environmental Laboratory/NOAA, Seattle Washington, USA

¹²Department of Atmospheric Sciences, University of Washington, Seattle, Washington, USA

¹³Cooperative Programs for the Advancement of Earth System Science, University Corporation for Atmospheric Research, Boulder, Colorado, USA

¹⁴Geophysical Fluid Dynamics Laboratory/NOAA, Princeton, New Jersey 08540-6649, USA.

¹⁵GEOMAR Helmholtz Centre for Ocean Research Duesternbrooker Weg 20, 24105 Kiel, Germany

¹⁶Department of Atmospheric Sciences, National Taiwan University, Taipei, Taiwan

¹⁷Department of Plants, Soils, and Climate, Utah State University, Utah, USA

¹⁸Centro de Estudios Avanzado en Zonas Áridas (CEAZA), Coquimbo, Chile. & Laboratoire d'Etudes en Géophysique et Océanographie Spatiale, Toulouse, France

¹⁹School of Earth, Atmosphere and Environment, Monash University, Clayton, Australia

²⁰Department of Earth and Environmental Sciences, University of Mary Washington, Fredericksburg, VA, USA

²¹Laboratoire d'Océanographie et du Climat: Expérimentation et Approches Numériques (LOCEAN), IRD/UPMC/CNRS/MNHN, Paris Cedex 05, France.

²²NCAS-Climate, University of Reading, Reading RG6 6BB, UK

²³Department of Oceanography, Chonnam National University, Gwangju, South Korea

²⁴Met Office Hadley Centre, FitzRoy Road, Exeter, EX1 3PB, U.K.

²⁵School of Urban and Environmental Engineering, Ulsan National Institute of Science and Technology, 44919, Ulsan, South Korea.

²⁶Climate Prediction Department, APEC Climate Center, Busan, Korea,

²⁷Australian Bureau of Meteorology, Melbourne, Australia

²⁸Laboratory for Climate Studies, National Climate Center, China Meteorological Administration, Beijing, China

²⁹ARC Centre of Excellence for Climate System Science, Faculty of Science, University of New South Wales, Sydney,
NSW 2052, AUSTRALIA

³⁰Instituto Geofísico del Perú, Lima, Peru

³¹University of Exeter College of Engineering, Mathematics and Physical Sciences, Exeter, UK

³²Institute of Oceanology, Chinese Academy of Sciences, Qingdao, P. R. China

³³Department of Marine Sciences and Convergent Technology, Hanyang University, Ansan, South Korea

³⁴School of Earth Sciences and Environmental Engineering, Gwangju Institute of Science and Technology, Gwangju,
61005, South Korea

³⁵CSIRO Ocean and Atmosphere, Hobart TAS 7001, Australia

*Correspondence to: Axel Timmermann. IBS Center for Climate Physics, Pusan National University,
Busan, Republic of Korea (E-mail: timmermann@pusan.ac.kr).

El Niño events are characterized by tropical Pacific surface warming and weakening of trade winds occurring every few years. Such conditions are accompanied by changes in atmospheric and oceanic circulation, affecting global climate, marine and terrestrial ecosystems, fisheries and human activities. The alternation of warm El Niño and cold La Niña conditions, referred to as the El Niño-Southern Oscillation (ENSO), represents the strongest year-to-year fluctuation of the global climate system. Here we provide a synthesis of our current understanding of the spatio-temporal complexity of this important climate mode and its influence on the earth system.

1) Introduction

Originally described in 1893 as “corriente del Niño”¹ – a warm regional ocean current that affected regional climate off the coast of Peru – the view on the El Niño phenomenon has changed over the past century. In the 1960s ENSO was recognized as a basin-scale phenomenon involving coupled atmosphere-ocean processes². A major international research program in the 1980s and 90s fundamentally advanced the ability to observe, understand and predict ENSO and its world-wide impacts³. During the past 20 years the understanding has continued to evolve as new layers of complexity (Box 1) were identified in ENSO dynamics and predictability. The concept of El Niño has developed from one of a canonical progression of phases from onset, maturity and demise⁴ (Figure 1) to one that accounts for its spatio-temporal complexity (Figure 2) and varying climatic impacts⁵⁻⁸ (Figure 3). We have also come to realize that

although ENSO primarily manifests itself as a year-to-year climate fluctuation, its dynamics involves a broad range of processes interacting on timescales from weeks^{9,10} to decades^{11,12}. This complexity introduces new challenges for seasonal forecasting.

The most recent El Niño¹³ in 2015/16 was initiated in boreal spring by a series of Westerly Wind Events (WWE) (Box 1, Figure 3e) – a form of weather noise. The associated wind forcing triggered downwelling oceanic Kelvin waves (Box 1, Figure 1), reducing the upwelling of cold subsurface waters in the Eastern Pacific Cold Tongue (Box 1) and leading to a central and eastern Pacific surface warming. The positive Sea Surface Temperature Anomaly (SSTA) shifted atmospheric convection from the Western Pacific Warm Pool (Box 1) to the central equatorial Pacific, causing a reduction in equatorial trade winds, which in turn intensified surface warming through the positive Bjerknes feedback (Box 1). The seasonally-paced termination of the 2015/16 event (Figure 3e) was associated with ocean dynamics and the slow discharge of equatorial heat into off-equatorial regions thus providing a delayed negative feedback (Box 1). The event started to decline in early 2016 and transitioned into a weak La Niña in mid 2016.

In broad terms this evolution is common to the other strong El Niño events in 1982/83 and 1997/98 (Figure 3c). However, no two events are alike – be they strong, moderate or weak (Figure 2, 3 f-m). This diversity arises from the varying roles of noise forcing (Figure 3c-e) and of positive and negative coupled atmosphere/ocean feedback processes¹⁴ (Box 1) that act to enhance and suppress growth of SST anomalies, respectively. The complexity of ENSO patterns, amplitude and temporal evolution – referred to as ENSO Complexity (Box 1) – along with internal atmospheric noise may also translate into a diversity of global impacts^{7,15}. When the underlying SSTs change in the equatorial Pacific, there are shifts in atmospheric deep convection, which in turn cause adjustments of the global Walker Circulation (Box 1) and generate stationary atmospheric waves¹⁶ that impact the far reaches of our planet. This perturbed global circulation influences weather variability leading to massive reorganizations of global temperature and rainfall patterns^{17,18} (Figure 3f-m).

Paleo-climate reconstructions of the ENSO phenomenon across the mid-late Holocene¹⁹

also show a wide range of amplitudes, thus highlighting the importance of internal climate processes in modulating ENSO's complexity on timescales ranging from decades to centuries. In addition, the activity of reconstructed ENSO variability shows an intensification in the late 20th Century relative to other pre-industrial periods^{19,20}, thus raising the general question of whether external forcings could influence ENSO's evolution and amplitude. How ENSO responds to greenhouse warming is one of the most compelling outstanding questions²¹.

Given the societal and environmental relevance of ENSO, it is paramount to improve our understanding of the processes that control ENSO's amplitude, timing, duration, predictability and global impacts. Here we synthesize our current understanding of ENSO dynamical processes and their role in controlling ENSO complexity. Against this backdrop we will highlight areas of uncertainty (section 6) as a stimulus for further research.

2) A conceptual view of ENSO dynamics

Early efforts to elucidate the dynamics of ENSO focused on the average (composite) evolution of El Niño events²², capturing the typical evolution of ocean and atmosphere conditions from early spring initiation of El Niño to a wintertime peak and transition to La Niña during the subsequent summer (Figure 1). The enhanced spectral interannual variability of ENSO (Figure 3a,b) has been explained by invoking positive atmosphere/ocean feedbacks and delayed negative ocean adjustment feedbacks (Box 1), which together can lead to oscillatory dynamics, as encapsulated by the delayed action oscillator²³ and recharge oscillator²⁴ modelling frameworks. In its most general form, the ENSO recharge oscillator model can be expressed as:

$$\begin{aligned} \frac{dT_e}{dt} &= I_{BJ}T_e + Fh \\ \frac{dh}{dt} &= -\varepsilon h - \alpha T_e, \end{aligned}$$

[equation (1)] where T_e and h represent the equatorial eastern Pacific surface temperature and zonal mean thermocline depth, respectively. The Bjerknes stability index I_{BJ} (referred to as the BJ index or ENSO linear growth rate; Figure 1j) depends on a

number of processes such as thermocline-, zonal advective- and Ekman-feedbacks to reinforce SST, and thermal advection by horizontal mean surface currents and thermal damping by net surface heat fluxes as negative feedbacks¹⁴ (Box 1). In equation (1) ε represents a damping rate of thermocline depth anomalies. The interannual timescale of the ENSO system is mainly determined by F and α , which capture the thermocline feedback (Box 1) and the slow equatorial recharge/discharge process (Box 1) associated with the oceanic heat transport, respectively. For constant I_{BJ} the model describes a linear recharge oscillator: Starting from neutral conditions $T_e \sim 0$ (typically in boreal winter-spring, Figure 1c, 2) and a charged thermocline state $h > 0$, an El Niño can grow (Figure 1d,e, 2). While eastern equatorial Pacific SSTA develop, the thermocline feedback (Box 1) Fh further intensifies the growth of SSTA by upwelling anomalously warm subsurface waters to the surface in the Eastern Pacific Cold Tongue. Moreover, positive eastern Pacific SSTA ($T_e > 0$) cause a weakening of the equatorial trade winds (Figure 1d,e). The associated wind-stress curl discharges the equatorial heat through Sverdrup transport (Box 1) and ocean boundary processes (Figure 1f). The resulting drainage of heat in turn weakens the thermocline feedback, and the ENSO recharge oscillator can transition into a La Niña state (Figure 1g,h), which is accompanied by a recharging of heat through opposite wind-stress curl anomalies (Figure 1h).

Comparing the linear oscillator solution of equation (1) ($I_{BJ} = \text{const}$) with the scatterplot of observed equatorial eastern Pacific temperature and zonal mean thermocline depth anomalies (Figure 2), we find substantial differences. The observed scatter diagram shows a high degree of irregularity and a notable positive skewness in eastern tropical Pacific SSTA towards El Niño events (Box 1, Figure 2). El Niño and La Niña events are very different in terms of their amplitude and time-evolution (Figure 1k, 2a). To account for this additional level of complexity the simple recharge oscillator model can be extended by including a nonlinear Bjerknes feedback term that represents either atmospheric or oceanic nonlinear processes²⁵ or multiplicative stochastic forcing²⁶ (Box 1). For these extensions, the recharge model can then simulate ENSO's skewed probability distribution (Figure 2) and the fast growth from neutral to strong El Niño conditions (Figure 1j). The observed positive skewness of SSTA (Figure 2), which indicates the importance of nonlinear dynamical and thermodynamical processes in the

coupled tropical Pacific climate system, implies that strong El Niño conditions, which typically last for 1 year, are on average shorter than La Niña events, which can persist for up to several years (Figure 1k).

Whereas conceptual models like equation (1) can simulate some key features of ENSO's evolution, they can neither explain the presence of ENSO's spatial diversity (Figure 3a,b,f-m), nor the potential remote effects of variability originating from the extra-tropical Pacific, Atlantic or Indian Ocean onto this diversity. An improved framework to characterize and explain ENSO complexity is needed to capture these aspects.

3) Space-time complexity of ENSO

In spite of some prominent commonalities discussed in section 2 (Figure 1), El Niño events differ considerably from each other in terms of magnitude, spatial pattern, temporal evolution, and predictability^{5-7,27} (Figure 2, 3 f-m). To characterize the leading modes of equatorial Pacific SST variability, and their diverse timescales, we conduct an Empirical Orthogonal Function (EOF) analysis of observed tropical Pacific SSTA²⁸ (Figure 3), which identifies the leading orthogonal patterns of variability. The leading EOF (Figure 3a), which corresponds to the classical El Niño pattern with eastern tropical Pacific warming, exhibits variability on quasi-quadrennial time scales (3-7 years) (spectral density estimate in Figure 3a). In contrast, the second EOF, which explains only 25% of the variance of the first mode, is characterized by an east/west zonal SST dipole in the tropical Pacific and has enhanced variance on quasi-biennial and decadal timescales (spectral density estimate Figure 3b). The interplay of these two EOFs largely captures the spatial diversity of the observed ENSO mode.

Some El Niño events (e.g. 1997/98) (Figure 3c,f) are characterized by pronounced warming in the Eastern Pacific (referred to as EP El Niño events), while others show a stronger positive projection on the second EOF mode, which leads to a more pronounced Central Pacific warming (referred to as CP El Niño events) (e.g. 2004/05) (Figure 3d,h,i,j). More generally, El Niño events can be viewed as the superposition of the two EOF modes, resulting in a continuum of ENSO flavors^{29,30} that capture a mix of EP and CP dynamics (e.g. 1991/92 and 2016/17 events) (Figure 2). La Niña events (e.g. 1999/2000) (Figure 3g), in addition to being weaker, exhibit less diversity in their

spatial patterns^{6,31}, thus clearly pointing to an asymmetry in the underlying dynamical processes for ENSO.

EP El Niño events (e.g. 1997/98) (Figure 3c) tend to involve basin-scale equatorial wind anomalies, a strong relaxation of the zonal tilt of the equatorial thermocline (Figure 1e), a more prominent role for the thermocline feedback (Box 1), large eastward shifts of tropical Pacific convection, and strong discharge of heat content (Figure 3c) from the equatorial region, which boosts the likelihood of transitioning into a La Niña event^{6,27}. In contrast, CP El Niño events (e.g. 2004/05) (Figure 3d) tend to involve more local wind feedbacks, a stronger role for the zonal advective feedback (Box 1), little reduction in the zonal tilt of the thermocline, weak shifts of convection, earlier termination, little poleward discharge of ocean heat content (Figure 3d), a stronger role for thermal damping (Box 1) during the decay phase, a reduced likelihood to transition into La Niña, and more susceptibility to disruption by wind noise^{6,27}. Compared to CP El Niños, strong EP El Niños also tend to terminate later in boreal spring, due to a trade wind collapse which suppresses the upwelling that normally connects the SST to the evolving thermocline depth³².

The spatial diversity in ENSO's SSTA patterns is also associated with different tropical precipitation patterns (Figure 3f-m), resulting in potentially different remote teleconnection patterns and corresponding weather and climate impacts^{7,33}. However, the length of the historical record is not sufficient to permit robust detection of differences in the impacts of the various El Niño flavors, given the high level of internal atmospheric variability³⁴. In addition to its spatial diversity, ENSO also exhibits substantial diversity in its temporal evolution (Figure 1k, 3 c,d,e).

Understanding this diversity of El Niño events is crucial for predicting ENSO's regional impacts, e.g. on precipitation patterns, tropical cyclones, and other severe weather⁵. The extent to which El Niño diversity is predictable relates to whether ENSO's complexity originates mainly from random processes, or from low-frequency deterministic dynamics. Random processes affecting a single physical ENSO mode could generate diversity in amplitude, spatial structure, and temporal evolution⁸, consistent with a spatial flavor continuum generated by different realizations of atmospheric noise²⁹.

Alternatively, initial subsurface ocean conditions could modulate the role of stochastic wind forcing in producing diversity. For example, climate model simulations have demonstrated that in the presence of stochastic WWEs, an initial buildup of equatorial Pacific upper-ocean heat content can favor the development of EP rather than CP El Niño events^{10,35,36} (Figure 3d,e). At the onset of strong El Niño events³⁷ such as 1997/98 and 2015/16 (Figure 3c,e), WWE activity tends to strengthen and expand eastward with the expansion of the Western Pacific Warm Pool and the relaxation of the trade winds. These WWE changes can be parameterized in equation (1) as multiplicative noise (Box 1), which can contribute to ENSO diversity and asymmetries^{9,38}.

Studies suggest that ENSO diversity may be triggered by climate phenomena outside the tropical Pacific, including the North³⁹ and South Pacific⁴⁰ meridional modes, extra-tropical atmospheric circulation patterns, and tropical Atlantic variability^{5,41,42}. For example, the negative phase of the North Pacific Oscillation⁴³ tends to favor the development of positive SST anomalies in the central Pacific by weakening the trade winds in the northern Hemisphere, while the positive phase of the South Pacific Oscillation tends to weaken the southern Hemisphere trades and favor the development of positive SSTAs in the eastern Pacific. Such remote influences appear to be mediated primarily by how they project onto wind variations in the equatorial Pacific. In essence, westerly wind anomalies in the western equatorial Pacific tend to favor CP El Niños, while westerly wind anomalies in the central-eastern equatorial Pacific tend to favor EP El Niños. These external influences can precede the peak of El Niño by 2-3 seasons^{41,43} and may provide additional predictability to the spatial characteristics of an emerging El Niño event.

Since 1998, CP events have been more prevalent than EP events⁴⁴. Such a decadal modulation in ENSO diversity is consistent with CGCMs that can spontaneously generate multidecadal variations in ENSO diversity even in the absence of external radiative forcings⁴⁵. Low-frequency climatic drivers (including natural and anthropogenic forcings) — which involve basinwide changes in the zonal SST gradient, thermocline depth, and winds^{46,47} — may also have contributed to the observed decadal swings in ENSO diversity by favoring particular spatio-temporal modes⁴⁸. At this stage,

the observational record remains too short to quantify all the possible sources of the decadal modulation of ENSO characteristics.

The current generation of climate models underestimates ENSO diversity⁴⁹. This issue is related to the models' systematic biases, which affect the mean state and ENSO feedbacks. Sources of these biases include deficiencies in the simulation of clouds, atmospheric convection, and oceanic mixing⁵⁰. In particular, atmospheric model responses tend to be relatively insensitive to distinct patterns of SST anomalies, due to climatological dry and cold biases in the equatorial central Pacific^{49,51}.

4) Seasonal ENSO dynamics

ENSO displays a close relationship with the seasonal cycle^{22,52}: El Niño events usually start in boreal spring (Figure 1c,i, 4), grow during the summer and fall (Figure 1d), reach their maximum intensity in winter (Figure 1e,i), and decay rapidly during late winter and spring (Figure 1f,j). In most cases, by the subsequent summer, they transition to La Niña events (Figure 1g,h, 4). This seasonal synchronization of ENSO translates into the observed eastern equatorial Pacific SSTA variance peaking during boreal winter and attaining minimum values during spring (Figure 1j). It also leads to pronounced seasonal contrasts in ENSO's climate impacts and predictability (Figure 1i). ENSO influences the global atmospheric circulation, affecting the Asian Monsoons⁵³, America⁵⁴, and Australia⁵⁵.

Randomly occurring sequences of WWEs, typically during spring, can lead to an initial warming of the central-eastern equatorial Pacific⁵⁶ (Figure 1c). This initial SSTA can grow because the air-sea coupling is strongest in summer and early fall^{57,58} (Figure 1j). Proposed physical processes for this summer/fall coupling maximum include (i) the equatorward shift of the ITCZ⁵⁹ and its associated increase in western Pacific surface wind convergence⁵⁹, (ii) the seasonal outcropping of the equatorial thermocline⁶⁰, (iii) the seasonal cooling of the eastern equatorial Pacific⁵⁹, (iv) and the reduction of the negative cloud feedbacks⁶¹.

The decay of El Niño events typically starts in boreal winter. The anomalous westerlies shift southward from the equator, leading to a shoaling of the eastern Pacific

thermocline, and a subsequent reduction of the overlying SSTA⁶² (Figure 1f, 4a). This shift arises from climatological expansion of the Western Pacific Warm Pool into the Southern Hemisphere, coincident with the development of the South Pacific Convergence Zone⁶³. In this season, the increased surface heat flux damping⁶¹ results in a decrease of the air-sea coupling strength (Figure 1j), which together with the aforementioned seasonal southward wind shift⁶⁴ and the equatorial heat content discharge²⁴ (Figure 4b) lead to a rapid transition to a La Niña state.

While these seasonal processes generally operate for different flavors and phases of ENSO, differences in their relative importance can contribute to ENSO complexity. For instance, CP events typically terminate earlier and are less likely to transition to a La Niña state compared to EP El Niño events⁶³ (Figure 3d). Furthermore, La Niña conditions can last up to 2-3 years (Figure 3c, 4b). The ability to simulate ENSO seasonal synchronization for different types of El Niño events varies strongly among the current generation of climate models, likely due to biases in mean state and seasonal cycle⁵⁷.

The influence of the seasonal variations of the air-sea coupling strength discussed above can be included in the framework of the recharge oscillator [equation (1)] by adding a seasonally varying growth rate (I_{BJ}). As expected, this model captures the observed ENSO seasonal synchronization characteristics, including the seasonal ENSO variance modulation and partial phase synchronization²⁵. Interactions between the seasonal cycle in I_{BJ} and the interannual ENSO temperature signal generate variance with periods at roughly 9 and 15-18 months, the so-called combination tone frequencies (Box 1) that broaden the ENSO spectrum predominantly towards higher frequencies^{65,66}. These interacting dynamics create specific atmospheric circulation patterns that are together referred to as Combination Mode⁶⁵ (C-mode) (Box 1). The spatial pattern of the C-mode exhibits a pronounced hemispheric asymmetry, which includes an anomalous cyclonic low-level wind circulation in the Southern Hemisphere Central Pacific and an anomalous anticyclonic low-level wind circulation in the Northern Hemisphere Western Pacific. Some of prominent local expressions are the aforementioned southward shift of equatorial wind anomalies⁶⁴ (Figure 1e) and the anomalous Western North Pacific Anticyclone⁶⁶.

5) ENSO predictability

To link our dynamical understanding of tropical air-sea interactions with ENSO predictability, it is helpful to elucidate the seasonal evolution of i) potential precursors that may contribute to long-term predictability⁶⁷ (15-9 months lead time), ii) triggers that can rapidly increase the likelihood for event development (9-6 months lead time) and iii) transition processes (section 2, 4). The development of a typical EP event can be divided into different seasonal stages which each contribute differently to the boreal winter Niño 3.4 SSTA forecasting skill of up to 9-6 months, as illustrated by the anomaly correlation coefficient skill between seasonal forecasts performed with the North American Multimodel Ensemble⁶⁸ (NMME) and the observations (Figure 4a, cyan dashed line). Prior to boreal spring a charged western tropical Pacific heat content is a necessary condition for the subsequent development of El Niño events (Figure 4 b). Corresponding warm pool heat advection processes^{69,70} thus play a key role in determining the long-term memory for ENSO forecasts. Furthermore, atmospheric precursors in the North³⁹ and South Pacific⁴⁰, the Indian Ocean⁷¹, or the tropical Atlantic^{42,72} have been suggested to influence the El Niño evolution for long lead times.

It must be emphasized here that the presence of such early oceanic or atmospheric precursors is not sufficient for El Niño growth, as one of the key trigger mechanisms is the stochastic WWE activity in boreal spring. Individual WWEs are not predictable beyond the weather prediction horizon, which implies that on average forecasts initialized in boreal spring have relatively low longterm skill⁷³ in particular in the absence of pre-cursor signals (Figure 4a, cyan line). However, pre-cursor signals in western tropical Pacific heat content (Figure 4b) could be indicative of potentially developing El Niño conditions, which in effect raises the predictability (Figure 4a, orange line), relative to the averaged case (Figure 4a, cyan line). The competing roles of stochasticity versus ocean memory for this so-called spring predictability barrier (Figure 4a) and for long-lead time forecasts have been intensely debated^{74,75}.

If a sufficient amount of westerly momentum is transferred in boreal spring from the atmosphere to the ocean, zonal advective processes begin moving the warm pool front eastward and downwelling Kelvin waves (Box 1) generate surface warming in the

eastern tropical Pacific about 2 months later. These anomalies will be further intensified (Figure 4a) owing to increasing summer air-sea coupling strength (Figure 1j), while anomalously warm water is drained from the Western Pacific Warm Pool (Figure 4b). This phase exhibits a high degree of climate predictability, as documented by the high anomaly correlation coefficients (>0.6) between predicted boreal winter El Niño events and observations for forecasts initialized in boreal summer (Figure 4a). The subsequent demise of an El Niño event is largely controlled by ocean-subsurface processes and the discharge of zonal heat content away from the equator (Figure 1i, 2), as well as by the seasonally modulated southward shift of westerly wind anomalies⁶⁴, which in turn leads to a relaxation of the zonally integrated thermocline anomalies. This seasonally locked decay of El Niño conditions under a low noise atmospheric environment further contributes to the long-term averaged ENSO prediction skill⁶³.

The subsequent evolution into a La Niña state (Figure 4a,b) and the possibility to have multi-year La Niña events (Figure 1k, 4c) are less well understood. La Niña events are often preceded by a strong El Niño. However, as indicated by the broad probability distribution of SSTA at lag 15-9 months (Figure 4c), other initial conditions can also develop into La Niña events peaking in boreal winter (Figure 4c). During the transition from El Niño to La Niña equatorial heat gets quickly discharged and 9-6 months prior to a peak La Niña in boreal winter, we observe the smallest values of the equatorial heat content (Figure 1i) and a slow recharging of the Western Pacific Warm Pool (Figure 4d). However, also during this period the probability density of western tropical Pacific heat content anomalies is relatively broad, which translates into an overall reduction of predictive skill (Figure 4c). As longer-lasting La Niña events are exposed to a variety of atmospheric and oceanic perturbations and the annual cycle, a dynamical decoupling of La Niña and subsequent El Niño events may occur⁷⁶. In boreal winter, during the peak of the La Niña, Western Pacific Warm Pool is fully charged (Figure 4d) to values that are typical for an El Niño pre-cursor (Figure 4b). However, the SST conditions do not necessarily have to swing back to an El Niño state and sometimes even a second subsequent La Niña can develop. Comparing the anomaly correlation coefficient skill for December La Niña target conditions with the averaged skill for all years (1980-2015) from the NMME⁶⁸, we find very little difference (Figure 4c) for lead times 12-1 month, which suggests i) that La Niña conditions have a considerably lower predictability than

El Niño, ii) the predictability of La Niña is to a first order captured well by the mean statistical skill of the current generation of seasonal prediction models. Using ensemble forecasting techniques, a recent study⁷⁷ identified potential predictors for the likelihood of multi-year La Niña events, which include the magnitude of thermocline discharge and the amplitude of the preceding El Niño event, suggesting the possibility for longer-term forecasts also for La Niña.

How the different stages of predictability differ between CP and EP events and whether there are distinct precursor patterns for different ENSO flavors still remains controversial^{69,78}. Despite an improved understanding of ENSO dynamics, ENSO prediction skill has not demonstrated a steady improvement during the past few decades, with even a decrease of ENSO prediction skill at the turn of the 21st Century⁷³. This decrease may be related to the reduced ENSO amplitude and the more frequent occurrence of CP events during that period⁷⁸, as their evolution and climate impacts tend to be less predictable than those of EP El Niño events⁷⁹.

6) A unifying framework

The discussions in previous sections have highlighted a variety of dynamical pathways that can be synthesized to explain the spatio-temporal complexity of the ENSO phenomenon (Figure 5). Extending beyond the simple single mode theory (section 2), which captures several features of ENSO dynamics, but not all, our proposed framework for ENSO complexity is based on the co-existence of a duplet of linear eigenmodes (Figure 5 a,b), which can be derived from a coupled intermediate ENSO model⁴⁸, and a number of excitation mechanisms. These two modes are characterized by spatial patterns that closely resemble the observed EP and CP modes (Figure 5) and by timescales of approximately 4 and 2 years, respectively. The 4-year (quasi-quadrennial, QQ) mode is more prominent (Figure 5, lower left) when the mean thermocline is deep and the tradewinds are weak. It relies strongly on the thermocline feedback. In contrast, the 2-year mode (quasi-biennial, QB) is dominant when the mean thermocline is shallow and the equatorial trade winds are strong. Its SST variability is strongly controlled by the zonal advective feedback⁴⁸. These features are akin to their observational counterparts (Figure 3, 5 c,d). For realistic background states both modes operate not far away from criticality (zero growth rate) (Figure 5, lower left), which

implies that they can be easily excited by other processes. Their stability and excitability depends further on the prevailing climatic background conditions.

At the heart of our explanation for ENSO's *spatial* flavors is the aforementioned multiplicity of coupled ENSO eigenmodes (Figure 5 a,b), as seen in intermediate ENSO models⁴⁸. Furthermore, the *temporal* complexity is generated in part by the different oscillation frequencies of the QQ and QB modes and additionally by different external excitation processes associated e.g. with the North and South Pacific Meridional Modes^{80,81}, the South Pacific booster⁴⁰, Westerly Wind Events (section 3,4), Tropical Instability Waves⁸², or transbasin influences^{42,83} (Figure 5). In particular, asymmetric dependencies related to the increased Westerly Wind event activity during El Niño and enhanced Tropical Instability Wave activity during La Niña make these cross scale interactions very effective sources for ENSO complexity. Furthermore, the annual cycle of winds and SST plays a key role in determining the seasonal timing of ENSO anomalies and its predictability (section 4). To further explain the fact that El Niño anomalies are stronger in amplitude (section 2) and exhibit a more pronounced spatial diversity (section 3), and higher predictability⁸⁴ relative to their La Niña counterparts (Figure 4,b,d, 5c,e), we need to invoke additional nonlinear processes. Nonlinearities, particularly in atmospheric deep convection and oceanic heat advection, can induce a wide range of additional timescales²⁵ and new spatial structures^{85,86} by potentially coupling and/or amplifying the primary ENSO modes.

Decadal subsurface processes^{87,88} can affect the long-term climatological background state. In turn this will change the stability of the two primary ENSO eigenmodes (Figure 5 a,b) and their excitability. Hence, slow background state changes in the Pacific Ocean can play a key role in generating and modulating ENSO's spatio-temporal complexity.

Our synthesis framework for ENSO complexity (Figure 5), which identifies key ingredients for ENSO complexity (primary ENSO eigenmodes, excitation processes, nonlinearities and cross-timescale interactions), may serve as a roadmap for further hypotheses testing, process studies and diagnostic analysis of climate models. It can help guide the evolution of the tropical Pacific observing system, which is an essential underpinning of ENSO research and forecasting⁸⁹. In addition, this framework can be

used to determine how the shortcomings in representing ENSO complexity in climate and earth system models are related to a variety of feedback processes and biases in the mean state and annual cycle that affect the generation of climate variability.

7) Outlook

The reliability of dynamical seasonal climate predictions depends heavily on the representation of ENSO processes in CGCMs. Climate models still exhibit stubborn climate biases in the eastern equatorial Pacific⁹⁰ that may impact their representation of feedbacks (section 2), ENSO complexity⁴⁹, and in turn may affect the fidelity of operational ENSO forecasts. Identifying and resolving underlying systematic model biases will help in developing the next generation of models for seamless climate forecasts and projections. Future research on ENSO complexity needs to address the role of the seasonal cycle for CP ENSO dynamics, the near-absence of spatial diversity for La Niña³¹ (Figure 5e), the impact of decadal background state changes on ENSO modes vis-à-vis multi-timescale processes involving Westerly Wind Events, Tropical Instability waves and extratropical triggers and the response of ENSO's spatio-temporal complexity to past and future climate change. Moreover, it needs to be studied, whether the underlying dynamical origin for spatial-temporal diversity in CGCMs can in fact be linked to the duplet of QQ and QB ENSO eigenmodes, described in section 6. This can be tested by applying interactive atmosphere ensemble averaging techniques in coupled climate models⁹¹, which artificially reduce non-SST-related atmospheric perturbations. Moreover, the use of flux-adjusted CGCMs⁹² could help elucidate how model biases impact ENSO's spatial diversity and provide a more effective way of improving seasonal climate predictions. Such experiments could further reveal if there are distinct precursors for ENSO diversity, which could be used to further inform ENSO forecasts. Much scientific emphasis has been placed on understanding the growth of El Niño events. However, given the severe impacts of La Niña e.g. on drought in the Southwestern United States⁹³ or the Horn of Africa⁹⁴, and the fact that La Niña events may last longer than one year (Figure 4), it will be paramount to gain also deeper understanding of the processes controlling La Niña and its predictability through observational, diagnostic and modeling studies.

A growing global population in the 21st century has become increasingly vulnerable to

natural hazards as human activities alter the climate and the environment. Society therefore has an urgent demand for better climate products and services, including improved seasonal ENSO predictions and long term projections, to better inform decision-making for agriculture and food security, public health, water resource management, energy production, human migration, and disaster risk reduction. ENSO is a unifying concept in earth system science⁹⁵. Thus, our proposed synthesis for ENSO complexity (sections 2-5) can serve as both a catalyst to further research and, in its practical applications, an essential contributor for sustainable development and environmental stewardship in a changing world.

Figure 1| ENSO Cycle: Composite evolution of El Niño events from 1958 to 2015. a) Mean sea surface temperature²⁸ (SST) and b) subsurface potential temperature⁹⁶ between 2°N and 2°S. The depth of the 20°C isotherm (Z20) is indicated by the black line. (c-h) Composite SST anomalies²⁸ (SSTA) and subsurface temperature anomalies⁹⁶ from 17 El Niño events (1963, 1965, 1968, 1969, 1972, 1976, 1977, 1982, 1986, 1987, 1991, 1994, 1997, 2002, 2004, 2006, 2009), based on the 0.5°C exceedance of the three month running mean of NOAA ERSST.v2 SST anomalies⁹⁷ in the Niño3.4 region (averaged over 5°S-5°N, 120°W-170°W). The arrows schematically represent wind anomalies and the boxes list major processes involved in the phases of El Niño evolution. (i) The composite means (lines) and spread (shading) of Niño3 SSTA (red, averaged over 5°S-5°N, 90°W-150°W,) and equatorial Pacific zonal mean Z20 (blue) for the 17 El Niño events. The diamond illustrates that ENSO predictability increases with increasing ENSO signal strength. (j) The monthly standard deviation (SD) of Niño3 SSTA²⁸ (red line) and an estimate of monthly ENSO growth rate based on the Bjerknes stability index⁵⁷. (k) Time series of Niño3 SSTA and zonal mean equatorial Pacific depth anomaly from 20°C isotherm (from 2°S-2°N, 120°E-80°W) from merged data product^{29,98}.

Figure 2: | Schematic representation of ENSO temporal complexity. Orange shading show the kernel density estimate of the joint probability distribution of linearly detrended Niño3 SSTA and zonal mean 20°C isotherm depth anomalies (from 2°S-2°N, 120°E-80°W) for the period 1958-2016 from a merged data product^{29,98}. The gray circles

indicate the monthly values of the two time series, smoothed with a 3-month running mean filter. Dark and light blue triangles indicate December values of EP (1972, 1982, 1986, 1997, 2006, 2015) and CP El Niños (1968, 1994, 2002, 2009). The years for the four largest El Niño events are indicated. The white ellipse in the center corresponds to the progression of the linear recharge oscillator, and arrows on the left and right indicate (dis)charging of subsurface warm water in the equatorial Pacific.

Figure 3. Spatio-temporal complexity of ENSO. 1st (a) 2nd (b) EOF patterns of linearly detrended SSTA⁹⁵ computed for 25°S-25°N, 140°E-80°W during 1920-2016, with associated variance-preserving spectral power density on the left (vertical axis is period in years, horizontal axis is log power); c,d,e) longitude-time evolution of Pacific SSTA averaged 5°S-5°N, for selected observed ENSO events, with 28.5°C isotherm of SST (red curve) representing the edge of the Western Pacific Warm Pool, longitude and strength of WWEs⁹⁹ (black circles), and (on the left) associated equatorial Pacific heat content anomaly (temperature anomaly averaged over the top 300 m of the ocean and between 5°S-5°N and 120°E-90°W; range from -1 to 1K; red positive, blue negative). The El Niño of 1997/98 exhibits initially strong heat content, a strong eastward expansion of the warm pool and WWE activity at El Niño onset in boreal spring and summer, and a strong reduction of heat content after the event. In contrast, the El Niño of 2004/05 shows weaker initial heat content, less eastward expansion of WWE activity, and almost no discharge of heat content⁹⁸ after the event. (f-m) spatial pattern of SSTA (shaded) and precipitation anomaly¹⁰⁰ (contours, positive solid, negative dashed, 2 mm/day interval, zero contour omitted) averaged over the Nov-Dec-Jan season of selected ENSO events. Note that strong warm events (1997/98, 2015/16) induce very strong eastward and equatorward shifts of rainfall. Bottom-right of each panel of (a,b,f-m) shows the associated principal components (PCs), namely the projection of each SSTA spatial pattern onto the EOF patterns in (a,b); abscissa is PC1, ordinate is PC2, and arrow length is relative to the unit circle.

Figure 4 | Probabilistic ENSO pre-cursors and predictive skill. Kernel-density probability density estimates of linearly detrended Niño3.4 SSTA²⁸ for the period 1958-2016 for a.) El Niño and b.) La Niña conditions, exceeding the +/-0.5°C threshold (White/transparent shading), respectively. c.) and d.) same as a.), b.), but for western

tropical Pacific heat content anomalies⁹⁶ (temperature anomalies averaged from 5°S-5°N, 120°E-155°W and 0-300 m and high-pass filtered with a cut-off period of 20 years to remove multi-decadal trends). The time-evolution of the probability density estimates is shown for different lead and lag times, relative to El Niño and La Niña events peaking in December. Colored thick lines correspond to the maximum probability for each lag. Thick lines in a.) represent the anomaly correlation coefficient skill (ACC) for December Niño3.4 SSTA⁹⁷ (1980-2015) exceeding +0.5°C (orange), within the range +/-0.5°C (gray) and for all years (cyan) as calculated using 9 coupled models from the North American Multimodel Ensemble project⁶⁸. Lines in b.), same as a.), but for anomalies below -0.5°C (blue), within the range +/-0.5°C (gray) and all years (cyan).

Figure 5 | Mechanisms for ENSO Complexity. Top two left panels: Leading modes of SSTA (°C) and equatorial thermocline depth anomalies (averaged between 5°S-5°N, unit in meters) with periods of ~4 (QQ) and ~2 (QB) year, as obtained from the eigenanalysis of an intermediate ENSO model⁴⁸. The differences in zonal location of the center in SSTA and thermocline anomalies are largely due to the different magnitude and spatial characteristics of the zonal advective feedback (ZAF) and thermocline feedback (TF). Bottom two panels on the left: growth rates (unit: 1/year) of the co-existing two leading ENSO modes as a functions of mean thermocline depth and the strength of mean equatorial trade winds relative to climatological conditions. The black dots mark the mean state condition for the modes displayed in the two panels above. Right panels: patterns of SSTA²⁸ and top 300m heat content anomalies (unit: 10¹⁰ J/m²) averaged between 5°S-5°N for typical EP (1997/98), CP (2009/2010) El Niño, and La Niña (boreal winter 2010) events (Nov-Dec-Jan) with schematic representation of key excitation, nonlinear and cross-scale interaction mechanisms: annual cycle (ACY), Westerly Wind Events (WWE), South Pacific Booster (SPB), North and South Pacific Meridional Modes (NPM, SPM) and Tropical Instability Waves (TIW). Note the similarity between observed (right) and theoretical (left) SSTA patterns and relative amplitude of feedbacks. The observations also exhibit a striking asymmetry between El Niño and La Niña spatial diversity, owing to the presence of nonlinear processes. ENSO complexity is also affected by decadal-scale changes of the equatorial background state, atmospheric influences originating from Indian Ocean and Atlantic Ocean SSTA, and

other external forcings. The solid red-eastward (blue-westward) arrows represent the ZAF and red-upward (blue-downward) TF for El Niño (La Niña) conditions, respectively. The relative sizes and different zonal positions of the arrows indicate qualitatively the strength and areas of strong feedback efficiency. Curly upward (downward) arrows denote the damping net surface heat flux feedback for El Niño (La Niña). Thermocline processes are characterized by heat content anomalies averaged over the upper 300 m in the right panels and depth anomalies of the 20°C isotherm in the left panels.

Box 1| ENSO Glossary:

Bjerknes feedback: Positive (reinforcing) ENSO feedback along the equator, in which a weakened equatorial zonal SST gradient weakens trade winds, which in turn further reduces the zonal SST gradient due to the balance of ocean dynamical and thermodynamical processes. The Bjerknes feedback is seasonally modulated and peaks in late boreal summer to fall. The Bjerknes feedback also tends to intensify the growth of La Niña events.

Combination Tones / C-mode: Enhanced spectral energy on timescales of 9 months and 15-18 months, generated by the nonlinear modulation of ENSO by the seasonal cycle, and vice versa. This interaction plays an important part in the seasonal turnabout of El Niño events and in establishing the linkage between ENSO and the East Asian Monsoon system.

Eastern Pacific Cold Tongue: An eastern equatorial Pacific region characterized by wind-driven upwelling of cold subsurface waters (Figure 1a,b). The Cold Tongue warms considerably during Eastern Pacific (EP) El Niño events, and cools during La Niña events. The subsiding branch of the atmospheric Walker Circulation is located over the Cold Tongue.

Ekman Feedback: Positive (negative) SST anomalies weaken (strengthen) the equatorial trade winds, reducing (increasing) the upwelling of cold subsurface water in the eastern equatorial Pacific, thus reinforcing the original SST anomaly.

ENSO Complexity: Complexity expands on the concept of ENSO “pattern diversity” to include also temporal characteristics, dynamics, predictability and global impacts. ENSO

638 complexity arises from processes operating on a variety of timescales (from weather,
639 annual cycle, interannual to decadal timescales).

640 **ENSO Skewness:** Amplitude asymmetry of El Niño and La Niña events, which quantifies
641 the fact that El Niño events attain larger amplitudes than La Niña events. Skewness is
642 clear indication of nonlinearity in the ENSO cycle.

643 **Equatorial Kelvin Wave:** Eastward propagating oceanic internal wave that displaces the
644 interface (thermocline) between warm surface waters and cold subsurface waters.
645 Westerly equatorial wind anomalies generate downwelling Kelvin waves, which deepen
646 the thermocline in the eastern Pacific and thus reduce the efficiency of cooling by
647 climatological upwelling in the eastern Pacific. The opposite occurs for easterly wind
648 anomalies. Kelvin waves need about 2 months to propagate across the equatorial
649 Pacific.

650 **Multiplicative Noise:** Interaction between Westerly Wind Events (WWEs) and
651 underlying SST in the western and central Pacific, in which warmer (colder) SST favors
652 more (fewer) WWEs, also referred to as state-dependent noise.

653 **Recharge/Discharge:** Meridional transport of heat into/out of equatorial band driven by
654 changes in near-equatorial wind variations. Recharge/discharge processes plays key
655 role in initiation and termination of El Niño events.

656 **Thermal damping:** Typically a negative feedback arising from SST-induced changes in
657 surface radiative and turbulent heat fluxes in the tropical Pacific. It involves tropical
658 clouds, convection and atmospheric boundary layer physics.

659 **Thermocline feedback:** Generally positive feedback operating in the eastern equatorial
660 Pacific, in which a warm (cold) equatorial SSTA weakens (strengthens) equatorial trade
661 winds, leading to mean upwelling of anomalously warm (cold) water.

662 **Westerly Wind Event:** Weather systems in the western and central Pacific, that are often
663 associated with an abrupt relaxation of the equatorial trade winds, generating
664 downwelling Kelvin waves and an eastward expansion of the Western Pacific Warm
665 Pool. WWEs play a central role in triggering and amplifying El Niño events.

666 **Western Pacific Warm Pool:** Some of the warmest waters in the worlds' oceans occur in
667 the western tropical Pacific with temperatures exceeding 28°C (Figure 1a,b). The Warm
668 Pool's seasonal north-south migrations and their influence on the atmosphere play an
669 important role in equatorial air-sea coupling, and in the termination of El Niño events.

670 **Zonal-advective feedback:** Positive feedback, particularly effective in the central Pacific,

in which a positive (negative) equatorial SSTA weakens (strengthens) equatorial trade winds, reducing (enhancing) the oceanic transport of cold waters from the eastern Pacific.

Acknowledgements:

AT, KJS, KSY, EZ were supported by the Institute for Basic Science (project code IBS-R028-D1). BD was funded by Fondecyt (grant 1151185). SIA was supported by Basic Science Research Program through National Research Foundation of Korea (NRF-2017R1A2A2A05069383). TB receives funding from SFB 754 "Climate-Biochemistry Interactions in the tropical Ocean". MJM is supported by NOAA. HLR is supported by China Meteorological Special Research Project (grant number: GYHY201506013). SI was supported by the UK-China Research & Innovation Partnership Fund through the Met Office Climate Science for Service Partnership (CSSP) China as part of the Newton Fund. MFS acknowledges support from NOAA Climate and Global Change Postdoctoral Fellowship Program, administered by UCAR's Cooperative Programs for the Advancement of Earth System Sciences (CPAESS). HR was partly funded by the National Environmental Science Program, Australia. This is PMEL contribution number 4723 and ICCP number 6.

- 1 Carrillo, C. N. Hidrografía oceánica. *Bol Soc Geogr Lima*, 72-110 (1893).
- 2 Bjerknes, J. Atmospheric Teleconnections from the Equatorial Pacific. *Monthly Weather Review* **97**, 163-172 (1969).
- 3 McPhaden, M. J., Busalacchi, A. J. & Anderson, D. L. T. A TOGA Retrospective. *Oceanography* **23**, 86-103, doi:10.5670/oceanog.2010.26 (2010).
- 4 Cai, W. J. *et al.* More extreme swings of the South Pacific convergence zone due to greenhouse warming. *Nature* **488**, 365-369, doi:10.1038/nature11358 (2012).
- 5 Capotondi, A. *et al.* Understanding ENSO Diversity. *Bulletin of the American Meteorological Society* **96**, 921-938, doi:10.1175/bams-d-13-00117.1 (2015).

- 703 6 Kug, J. S., Jin, F. F. & An, S. I. Two Types of El Niño Events: Cold Tongue El Niño
704 and Warm Pool El Niño. *Journal of Climate* **22**, 1499-1515,
705 doi:10.1175/2008jcli2624.1 (2009).
- 706 **Demonstrates that the two types of El Niño (CP and EP) have different dynamical**
707 **structures including discharge processes and dominant SST feedbacks.**
- 708 7 Ashok, K., Behera, S. K., Rao, S. A., Weng, H. Y. & Yamagata, T. El Niño Modoki and
709 its possible teleconnection. *Journal of Geophysical Research-Oceans* **112**,
710 doi:10.1029/2006jc003798 (2007).
- 711 8 Takahashi, K., Montecinos, A., Goubanova, K. & Dewitte, B. ENSO regimes:
712 Reinterpreting the canonical and Modoki El Niño. *Geophysical Research Letters*
713 **38**, doi:10.1029/2011gl047364 (2011).
- 714 9 Tziperman, E. & Yu, L. S. Quantifying the dependence of westerly wind bursts on
715 the large-scale tropical Pacific SST. *Journal of Climate* **20**, 2760-2768,
716 doi:10.1175/jcli4138.1 (2007).
- 717 10 Lengaigne, M. *et al.* Triggering of El Niño by westerly wind events in a coupled
718 general circulation model. *Climate Dynamics* **23**, 601-620, doi:10.1007/s00382-
719 004-0457-2 (2004).
- 720 11 Timmermann, A. Decadal ENSO amplitude modulations: a nonlinear paradigm.
721 *Global and Planetary Change* **37**, 135-156, doi:10.1016/S0921-8181(02)00194-7
722 (2003).
- 723 12 Choi, J., An, S. I. & Yeh, S. W. Decadal amplitude modulation of two types of ENSO
724 and its relationship with the mean state. *Climate Dynamics* **38**, 2631-2644,
725 doi:10.1007/s00382-011-1186-y (2012).
- 726 13 L'Heureux, M. L. *et al.* Observing and predicting the 2015/16 El Niño. *Bulletin of*
727 *the American Meteorological Society* **98**, 1363-1382, doi:10.1175/bams-d-16-
728 0009.1 (2017).
- 729 14 Jin, F. F., Kim, S. T. & Bejarano, L. A coupled-stability index for ENSO. *Geophysical*
730 *Research Letters* **33**, doi:10.1029/2006gl027221 (2006).
- 731 15 Hoerling, M. P. & Kumar, A. Why do North American climate anomalies differ
732 from one El Niño event to another? *Geophysical Research Letters* **24**, 1059-1062,
733 doi:10.1029/97gl00918 (1997).
- 734 16 Karoly, D. J. & Hoskins, B. J. 3 dimensional Propagation of Planetary Waves.
735 *Journal of the Meteorological Society of Japan* **60**, 109-123 (1982).

- 736 17 Ropelewski, C. F. & Halpert, M. S. Global and Regional Scale Precipitation
737 Patterns associated with the El-Niño Southern Oscillation. *Monthly Weather*
738 *Review* **115**, 1606-1626, (1987).
- 739 18 Larkin, N. K. & Harrison, D. E. On the definition of El Niño and associated
740 seasonal average US weather anomalies. *Geophysical Research Letters* **32**, 4,
741 doi:10.1029/2005gl022738 (2005).
- 742 19 Cobb, K. M. *et al.* Highly Variable El Niño-Southern Oscillation Throughout the
743 Holocene. *Science* **339**, 67-70, doi:10.1126/science.1228246 (2013).
- 744 20 McGregor, S., Timmermann, A., England, M. H., Timm, O. E. & Wittenberg, A. T.
745 Inferred changes in El Niño-Southern Oscillation variance over the past six
746 centuries. *Climate of the Past* **9**, 2269-2284, doi:10.5194/cp-9-2269-2013
747 (2013).
- 748 **Documents using multi-proxy data that ENSO variance has increased over the past**
749 **Century, relative to the 500 years prior to this.**
- 750 21 Cai, W. J. *et al.* ENSO and greenhouse warming. *Nature Climate Change* **5**, 849-
751 859, doi:10.1038/nclimate2743 (2015).
- 752 22 Rasmusson, E. M. & Carpenter, T. H. Variations in Tropical Sea-Surface
753 Temperature and Surface Wind Fields associated with the Southern Oscillation
754 El-Niño. *Monthly Weather Review* **110**, 354-384, (1982).
- 755 23 Battisti, D. S. & Hirst, A. C. Interannual Variability in a Tropical Atmosphere
756 Ocean Model - Influence of the Basic State, Ocean Geometry and Nonlinearity.
757 *Journal of the Atmospheric Sciences* **46**, 1687-1712, (1989).
- 758 24 Jin, F. F. An equatorial ocean recharge paradigm for ENSO. Part I: Conceptual
759 model. *Journal of the Atmospheric Sciences* **54**, 811-829, (1997).
- 760 **Introduces heuristic model that explains key features of ENSO dynamics, such as the**
761 **important role of recharge and discharge processes in ENSO.**
- 762 25 Roberts, A., Guckenheimer, J., Widiastih, E., Timmermann, A. & Jones, C. Mixed-
763 Mode Oscillations of El Niño-Southern Oscillation. *Journal of the Atmospheric*
764 *Sciences* **73**, 1755-1766, doi:10.1175/jas-d-15-0191.1 (2016).
- 765 26 Levine, A. F. Z. & Jin, F. F. Noise-Induced Instability in the ENSO Recharge
766 Oscillator. *Journal of the Atmospheric Sciences* **67**, 529-542,
767 doi:10.1175/2009jas3213.1 (2010).

- 768 27 Kao, H. Y. & Yu, J. Y. Contrasting Eastern-Pacific and Central-Pacific Types of
769 ENSO. *Journal of Climate* **22**, 615-632, doi:10.1175/2008jcli2309.1 (2009).
- 770 28 Rayner, N. A. *et al.* Global analyses of sea surface temperature, sea ice, and night
771 marine air temperature since the late nineteenth century. *Journal of Geophysical*
772 *Research-Atmospheres* **108**, 4407, doi:10.1029/2002jd002670 (2003).
- 773 29 Giese, B. S. & Ray, S. El Niño variability in simple ocean data assimilation (SODA),
774 1871-2008. *Journal of Geophysical Research-Oceans* **116**,
775 doi:10.1029/2010jc006695 (2011).
- 776 30 Johnson, N. C. How Many ENSO Flavors Can We Distinguish? *Journal of Climate*
777 **26**, 4816-4827, doi:10.1175/jcli-d-12-00649.1 (2013).
- 778 31 Kug, J. S. & Ham, Y. G. Are there two types of La Niña? *Geophysical Research*
779 *Letters* **38**, doi:10.1029/2011gl048237 (2011).
- 780 32 Lengaigne, M. & Vecchi, G. A. Contrasting the termination of moderate and
781 extreme El Niño events in coupled general circulation models. *Climate Dynamics*
782 **35**, 299-313, doi:10.1007/s00382-009-0562-3 (2010).
- 783 33 An, S.-I., Kug, J.-S., Timmermann, A., Kang, I.-S. & Timm, O. The influence of ENSO
784 on the generation of decadal variability in the North Pacific. *Journal of Climate*
785 **20**, 667-680, doi:10.1175/JCLI4017.1 (2007).
- 786 34 Deser, C., Simpson, I. R., McKinnon, K. A. & Phillips, A. S. The Northern
787 Hemisphere Extratropical Atmospheric Circulation Response to ENSO: How Well
788 Do We Know It and How Do We Evaluate Models Accordingly? *Journal of Climate*
789 **30**, 5059-5082, doi:10.1175/jcli-d-16-0844.1 (2017).
- 790 35 Fedorov, A. V., Hu, S. N., Lengaigne, M. & Guilyardi, E. The impact of westerly
791 wind bursts and ocean initial state on the development, and diversity of El Niño
792 events. *Climate Dynamics* **44**, 1381-1401, doi:10.1007/s00382-014-2126-4
793 (2015).
- 794 36 Chen, D. K. *et al.* Strong influence of westerly wind bursts on El Niño diversity.
795 *Nature Geoscience* **8**, 339-345, doi:10.1038/ngeo2399 (2015).
- 796 37 Seiki, A. & Takayabu, Y. N. Westerly wind bursts and their relationship with
797 intraseasonal variations and ENSO. Part I: Statistics. *Monthly Weather Review*
798 **135**, 3325-3345, doi:10.1175/mwr3477.1 (2007).

799 38 Jin, F. F., Lin, L., Timmermann, A. & Zhao, J. Ensemble-mean dynamics of the
800 ENSO recharge oscillator under state-dependent stochastic forcing. *Geophysical*
801 *Research Letters* **34**, L03807, doi:10.1029/2006gl027372 (2007).

802 39 Vimont, D. J., Battisti, D. S. & Hirst, A. C. The seasonal footprinting mechanism in
803 the CSIRO general circulation models. *Journal of Climate* **16**, 2653-2667, (2003).

804 **Presents a coupled air-sea mechanisms by which extratropical Pacific climate anomalies**
805 **can propagate into the tropics**

806 40 Hong, L. C., LinHo & Jin, F. F. A Southern Hemisphere booster of super El Niño.
807 *Geophysical Research Letters* **41**, 2142-2149, doi:10.1002/2014gl059370
808 (2014).

809 41 Ham, Y. G., Kug, J. S., Park, J. Y. & Jin, F. F. Sea surface temperature in the north
810 tropical Atlantic as a trigger for El Niño/Southern Oscillation events. *Nature*
811 *Geoscience* **6**, 112-116, doi:10.1038/ngeo1686 (2013).

812 42 Chikamoto, Y. *et al.* Skilful multi-year predictions of tropical trans-basin climate
813 variability. *Nature Communications* **6**, doi:10.1038/ncomms7869 (2015).

814 **Documents the impact of Atlantic SST anomalies on the generation of CP El Niño events**

815 43 Yu, J. Y. & Kim, S. T. Relationships between Extratropical Sea Level Pressure
816 Variations and the Central Pacific and Eastern Pacific Types of ENSO. *Journal of*
817 *Climate* **24**, 708-720, doi:10.1175/2010jcli3688.1 (2011).

818 44 Lee, T. & McPhaden, M. J. Increasing intensity of El Niño in the central-equatorial
819 Pacific. *Geophysical Research Letters* **37**, doi:10.1029/2010gl044007 (2010).

820 45 Wittenberg, A. T., Rosati, A., Delworth, T. L., Vecchi, G. A. & Zeng, F. R. ENSO
821 Modulation: Is It Decadally Predictable? *Journal of Climate* **27**, 2667-2681,
822 doi:10.1175/jcli-d-13-00577.1 (2014).

823 46 Yeh, S. W. *et al.* El Niño in a changing climate. *Nature* **461**, 511-514,
824 doi:10.1038/nature08316 (2009).

825 47 Capotondi, A. & Sardeshmukh, P. D. Optimal precursors of different types of
826 ENSO events. *Geophysical Research Letters* **42**, 9952-9960,
827 doi:10.1002/2015gl066171 (2015).

828 48 Xie, R. & Jin, F.-F. Two Leading ENSO Modes and El Niño Types in the Zebiak-
829 Cane Model *Journal of Climate*, doi:10.1175/JCLI-D-1117-0469.1 (2018).

830 **Theoretical evidence for two coupled modes which resemble EP and CP El Niño events**
831 **with different timescales and background state sensitivities**

832 49 Ham, Y. G. & Kug, J. S. How well do current climate models simulate two types of
833 El Niño? *Climate Dynamics* **39**, 383-398, doi:10.1007/s00382-011-1157-3
834 (2012).

835 **Shows that the current generation of climate models tends to underestimate diversity of**
836 **El Niño due dry and cold biases in the equatorial central Pacific**

837 50 Bellenger, H., Guilyardi, E., Leloup, J., Lengaigne, M. & Vialard, J. ENSO
838 representation in climate models: from CMIP3 to CMIP5. *Climate Dynamics* **42**,
839 1999-2018, doi:10.1007/s00382-013-1783-z (2014).

840 51 Bayr, T. *et al.* Mean-state dependence of ENSO atmospheric feedbacks in climate
841 models. *Climate Dynamics*, doi:10.1007/s00382-00017-03799-00382 (2017).

842 52 Li, T. Phase transition of the El Niño Southern oscillation: A stationary SST mode.
843 *Journal of the Atmospheric Sciences* **54**, 2872-2887 (1997).

844 **Applies seasonally varying instability to model of coupled ENSO dynamics.**

845 53 Zhang, W. J. *et al.* Unraveling El Niño's impact on the East Asian Monsoon and
846 Yangtze River summer flooding. *Geophysical Research Letters* **43**, 11375-11382,
847 doi:10.1002/2016gl071190 (2016).

848 54 Trenberth, K. E. *et al.* Progress during TOGA in understanding and modeling
849 global teleconnections associated with tropical sea surface temperatures. *Journal*
850 *of Geophysical Research-Oceans* **103**, 14291-14324, doi:10.1029/97jc01444
851 (1998).

852 55 Risbey, J. S., Pook, M. J., McIntosh, P. C., Wheeler, M. C. & Hendon, H. H. On the
853 Remote Drivers of Rainfall Variability in Australia. *Monthly Weather Review* **137**,
854 3233-3253, doi:10.1175/2009mwr2861.1 (2009).

855 56 Vecchi, G. A. & Harrison, D. E. Tropical Pacific sea surface temperature anomalies,
856 El Niño, and equatorial westerly wind events. *Journal of Climate* **13**, 1814-1830,
857 (2000).

858 57 Wengel, C., Latif, M., Park, W., Harlass, J. & Bayr, T. Seasonal ENSO phase locking
859 in the Kiel Climate Model: The importance of the equatorial cold sea surface
860 temperature bias. *Climate Dynamics*, doi:10.1007/s00382-00017-03648-00383
861 (2017).

862 58 Zebiak, S. E. & Cane, M. A. A Model El-Niño Southern Oscillation. *Monthly*
863 *Weather Review* **115**, 2262-2278, (1987).

- 864 59 Tziperman, E., Zebiak, S. E. & Cane, M. A. Mechanisms of seasonal - ENSO
865 interaction. *Journal of the Atmospheric Sciences* **54**, 61-71, (1997).
- 866 60 Galanti, E. *et al.* The equatorial thermocline outcropping - A seasonal control on
867 the tropical Pacific Ocean-atmosphere instability strength. *Journal of Climate* **15**,
868 2721-2739, (2002).
- 869 61 Dommenges, D. & Yu, Y. S. The seasonally changing cloud feedbacks contribution
870 to the ENSO seasonal phase-locking. *Climate Dynamics* **47**, 3661-3672,
871 doi:10.1007/s00382-016-3034-6 (2016).
- 872 62 Harrison, D. E. & Vecchi, G. A. On the termination of El Niño. *Geophysical*
873 *Research Letters* **26**, 1593-1596, doi:10.1029/1999gl900316 (1999).
- 874 63 Lengaigne, M., Boulanger, J. P., Menkes, C. & Spencer, H. Influence of the seasonal
875 cycle on the termination of El Niño events in a coupled general circulation model.
876 *Journal of Climate* **19**, 1850-1868, doi:10.1175/jcli3706.1 (2006).
- 877 64 McGregor, S., Timmermann, A., Schneider, N., Stuecker, M. F. & England, M. H. The
878 Effect of the South Pacific Convergence Zone on the Termination of El Niño
879 Events and the Meridional Asymmetry of ENSO. *Journal of Climate* **25**, 5566-
880 5586, doi:10.1175/jcli-d-11-00332.1 (2012).
- 881 **Demonstrates that the southward wind-shift that leads to rapid decay of El Niño events is**
882 **related to the seasonal formation of the South Pacific Convergence Zone**
- 883 65 Stuecker, M. F., Timmermann, A., Jin, F. F., McGregor, S. & Ren, H. L. A
884 combination mode of the annual cycle and the El Niño/Southern Oscillation.
885 *Nature Geoscience* **6**, 540-544, doi:10.1038/ngeo1826 (2013).
- 886 66 Stuecker, M. F., Jin, F. F., Timmermann, A. & McGregor, S. Combination Mode
887 Dynamics of the Anomalous Northwest Pacific Anticyclone. *Journal of Climate* **28**,
888 1093-1111, doi:10.1175/jcli-d-14-00225.1 (2015).
- 889 67 Meinen, C. S. & McPhaden, M. J. Observations of warm water volume changes in
890 the equatorial Pacific and their relationship to El Niño and La Niña. *Journal of*
891 *Climate* **13**, 3551-3559, (2000).
- 892 68 Barnston, A. G. & Tippett, M. K. Do Statistical Pattern Corrections Improve
893 Seasonal Climate Predictions in the North American Multimodel Ensemble
894 Models? *Journal of Climate* **30**, 8335-8355, doi:10.1175/jcli-d-17-0054.1 (2017).
- 895 69 Ramesh, N. & Murtugudde, R. All flavours of El Niño have similar early
896 subsurface origins. *Nature Climate Change* **3**, 42-46 (2013).

- 897 70 Ballester, J., Bordoni, S., Petrova, D. & Rodo, X. Heat advection processes leading
898 to El Niño events as depicted by an ensemble of ocean assimilation products.
899 *Journal of Geophysical Research-Oceans* **121**, 3710-3729,
900 doi:10.1002/2016jc011718 (2016).
- 901 71 Izumo, T. *et al.* Influence of the state of the Indian Ocean Dipole on the following
902 year's El Niño. *Nature Geoscience* **3**, 168-172, doi:10.1038/ngeo760 (2010).
- 903 72 Ham, Y. G., Kug, J. S. & Park, J. Y. Two distinct roles of Atlantic SSTs in ENSO
904 variability: North Tropical Atlantic SST and Atlantic Niño. *Geophysical Research*
905 *Letters* **40**, 4012-4017, doi:10.1002/grl.50729 (2013).
- 906 73 Barnston, A. G., Tippett, M. K., L'Heureux, M. L., Li, S. H. & DeWitt, D. G. Skill of
907 Real-Time Seasonal ENSO Model Predictions during 2002-11: Is Our Capability
908 Increasing? *Bulletin of the American Meteorological Society* **93**, 631-651,
909 doi:10.1175/bams-d-11-00111.1 (2012).
- 910 74 Newman, M. & Sardeshmukh, P. D. Are we near the predictability limit of tropical
911 Indo-Pacific sea surface temperatures? *Geophysical Research Letters* **44**, 8520-
912 8529, doi:10.1002/2017gl074088 (2017).
- 913 75 Petrova, D., Koopman, S. J., Ballester, J. & Rodo, X. Improving the long-lead
914 predictability of El Niño using a novel forecasting scheme based on a dynamic
915 components model. *Climate Dynamics* **48**, 1249-1276, doi:10.1007/s00382-016-
916 3139-y (2017).
- 917 76 Kessler, W. S. Is ENSO a cycle or a series of events? *Geophysical Research Letters*
918 **29**, doi:10.1029/2002gl015924 (2002).
- 919 **Challenges the notion of ENSO as a cycle and highlights the fact that the ENSO system can**
920 **lose its dynamical memory during long La Niña events**
- 921 77 DiNezio, P. N., Deser, C., Okumura, Y. & Karspeck, A. Predictability of 2-year La
922 Niña events in a coupled general circulation model. *Climate Dynamics* **49**, 4237-
923 4261, doi:10.1007/s00382-017-3575-3 (2017).
- 924 78 McPhaden, M. J. A 21st century shift in the relationship between ENSO SST and
925 warm water volume anomalies. *Geophysical Research Letters* **39**,
926 doi:10.1029/2012gl051826 (2012).
- 927 79 Jeong, H. I. *et al.* Assessment of the APCC coupled MME suite in predicting the
928 distinctive climate impacts of two flavors of ENSO during boreal winter. *Climate*
929 *Dynamics* **39**, 475-493, doi:10.1007/s00382-012-1359-3 (2012).

930 80 Larson, S. & Kirtman, B. The Pacific Meridional Mode as a trigger for ENSO in a
931 high-resolution coupled model. *Geophysical Research Letters* **40**, 3189-3194,
932 doi:10.1002/grl.50571 (2013).

933 81 Zhang, H. H., Clement, A. & Di Nezio, P. The South Pacific Meridional Mode: A
934 Mechanism for ENSO-like Variability. *Journal of Climate* **27**, 769-783,
935 doi:10.1175/jcli-d-13-00082.1 (2014).

936 82 An, S. I. Interannual variations of the Tropical Ocean instability wave and ENSO.
937 *Journal of Climate* **21**, 3680-3686, doi:10.1175/2008jcli1701.1 (2008).

938 83 Okumura, Y. M. & Deser, C. Asymmetry in the Duration of El Niño and La Niña.
939 *Journal of Climate* **23**, 5826-5843, doi:10.1175/2010jcli3592.1 (2010).

940 84 Larson, S. M. & Kirtman, B. P. Linking preconditioning to extreme ENSO events
941 and reduced ensemble spread. *Climate Dynamics*, doi:10.1007/s00382-00017-
942 03791-x (2017).

943 85 Chen, N. & Majda, A. J. Simple dynamical models capturing the key features of the
944 Central Pacific El Niño. *Proceedings of the National Academy of Sciences of the*
945 *United States of America* **113**, 11732-11737, doi:10.1073/pnas.1614533113
946 (2016).

947 86 Hao, Z., Neelin, J. D. & Jin, F. F. Nonlinear Tropical Air-Sea Interaction in the Fast-
948 Wave Limit. *Journal of Climate* **6**, 1523-1544, (1993).

949 87 Schneider, N. The response of tropical climate to the equatorial emergence of
950 spiciness anomalies. *Journal of Climate* **17**, 1083-1095, (2004).

951 88 McGregor, S., Sen Gupta, A., Holbrook, N. J. & Power, S. B. The Modulation of ENSO
952 Variability in CCSM3 by Extratropical Rossby Waves. *Journal of Climate* **22**, 5839-
953 5853, doi:10.1175/2009jcli2922.1 (2009).

954 89 Xue, Y. *et al.* A real-time ocean reanalyses intercomparison project in the context
955 of Tropical Pacific observing system and ENSO monitoring. *Climate Dynamics* **49**,
956 3647-3672, doi:10.1007/s00382-017-3535-y (2017).

957 90 Widlansky, M. J. *et al.* Changes in South Pacific rainfall bands in a warming
958 climate. *Nature Climate Change* **3**, 417-423, doi:10.1038/NCLIMATE1726
959 (2013).

960 91 Kirtman, B. P., Straus, D. M., Min, D. H., Schneider, E. K. & Siqueira, L. Toward
961 linking weather and climate in the interactive ensemble NCAR climate model.
962 *Geophysical Research Letters* **36**, doi:10.1029/2009gl038389 (2009).

963 92 Vecchi, G. A. *et al.* On the Seasonal Forecasting of Regional Tropical Cyclone
964 Activity. *Journal of Climate* **27**, 7994-8016, doi:10.1175/jcli-d-14-00158.1
965 (2014).

966 93 Cook, E. R., Seager, R., Cane, M. A. & Stahle, D. W. North American drought:
967 Reconstructions, causes, and consequences. *Earth-Science Reviews* **81**, 93-134,
968 doi:10.1016/j.earscirev.2006.12.002 (2007).

969 94 Nicholson, S. E. & Selato, J. C. The influence of La Niña on African rainfall.
970 *International Journal of Climatology* **20**, 1761-1776, (2000).

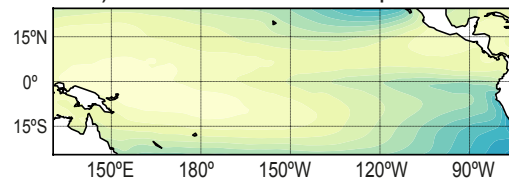
971 95 McPhaden, M. J., Zebiak, S. E. & Glantz, M. H. ENSO as an integrating concept in
972 Earth science. *Science* **314**, 1740-1745, doi:10.1126/science.1132588 (2006).

973 96 Balmaseda, M. A., Mogensen, K. & Weaver, A. T. Evaluation of the ECMWF ocean
974 reanalysis system ORAS4. *Quarterly Journal of the Royal Meteorological Society*
975 **139**, 1132-1161, doi:10.1002/qj.2063 (2013).

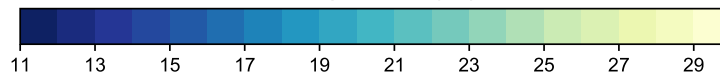
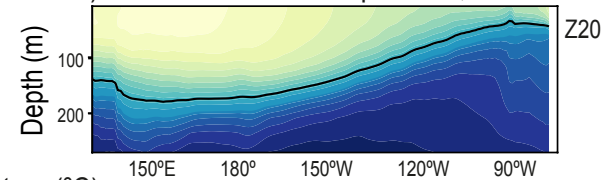
976 97 Huang, B. Y. *et al.* Extended Reconstructed Sea Surface Temperature, Version 5
977 (ERSSTv5): Upgrades, Validations, and Intercomparisons. *Journal of Climate* **30**,
978 8179-8205, doi:10.1175/jcli-d-16-0836.1 (2017).

979 98 Penny, S. G., Behringer, D. W., Carton, J. A. & Kalnay, E. A Hybrid Global Ocean
980 Data Assimilation System at NCEP. *Monthly Weather Review* **143**, 4660-4677,
981 doi:10.1175/mwr-d-14-00376.1 (2015).
982

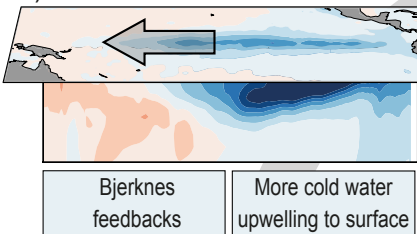
a) Mean sea surface temperature



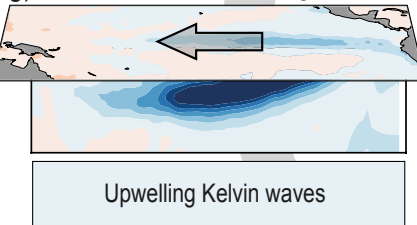
b) Mean subsurface temperature, 2°S-2°N



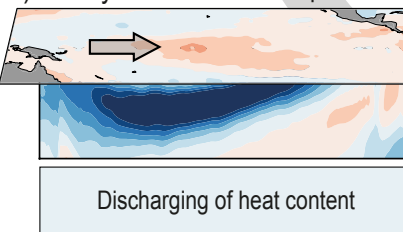
h) Mature La Niña December Year 1



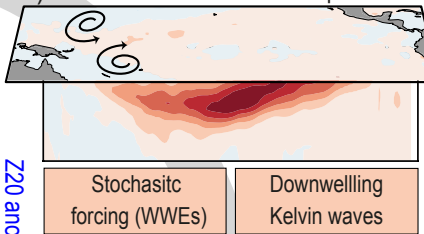
g) Transition August Year 1



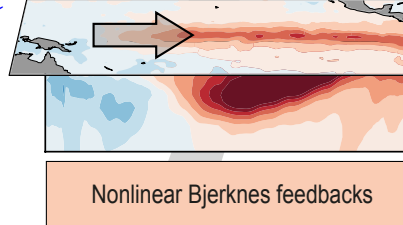
f) Decay April Year 1



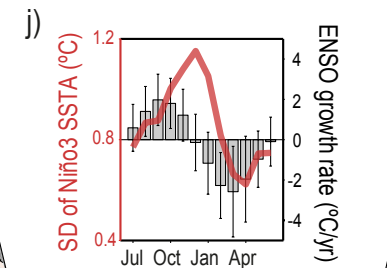
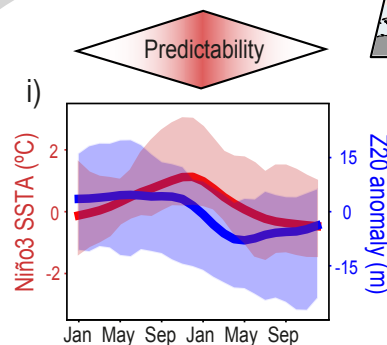
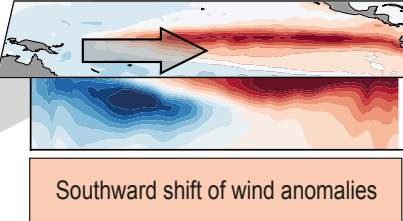
c) Onset April Year 0



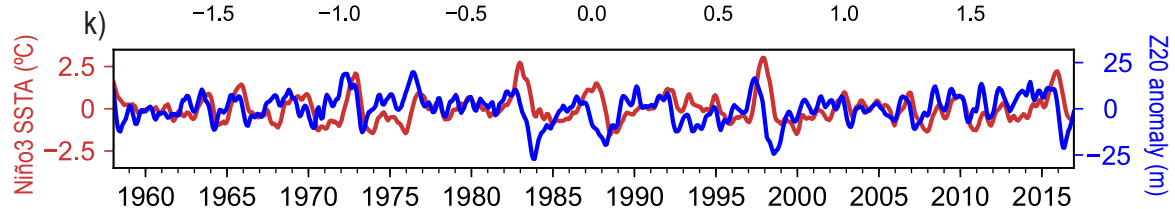
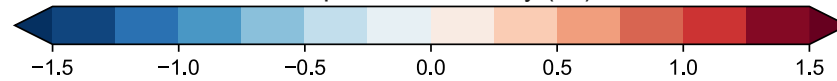
d) Growth August Year 0

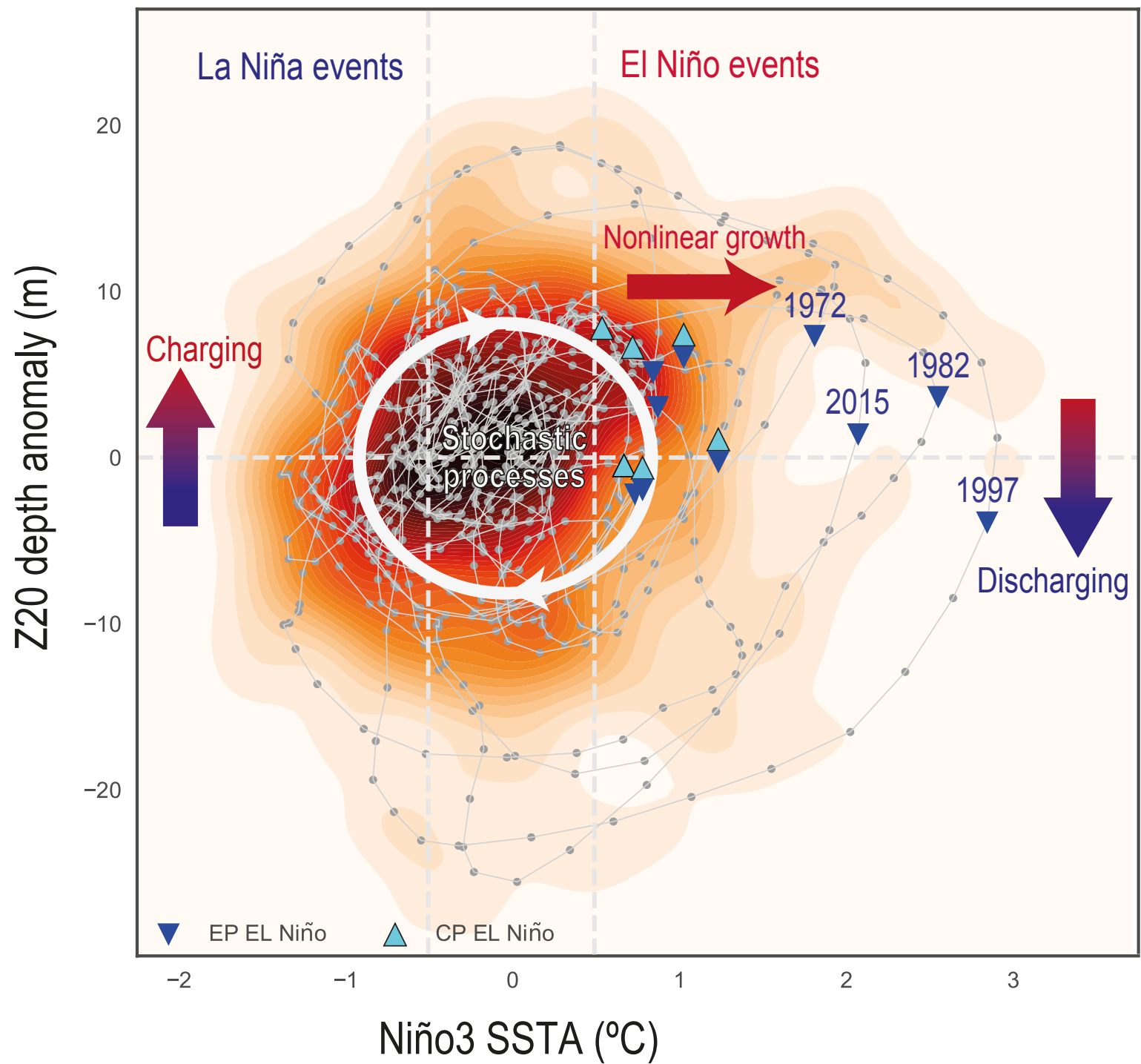


e) Mature El Niño December Year 0

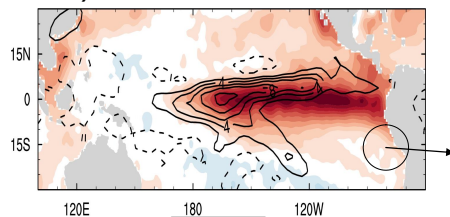


Temperature anomaly (°C)

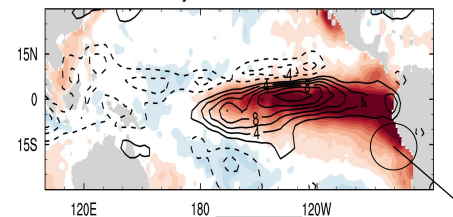




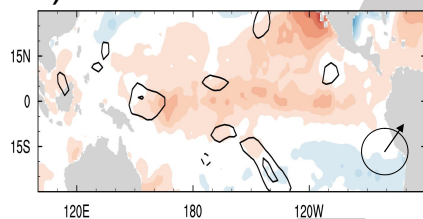
m) 2015/16 EN



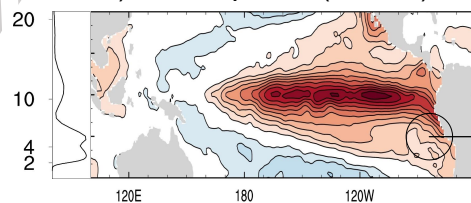
f) 1997/98 EN



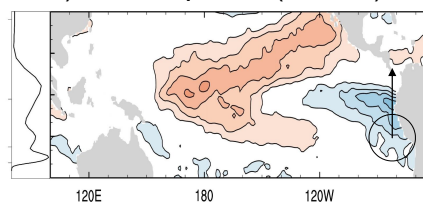
l) 2014/15 EN



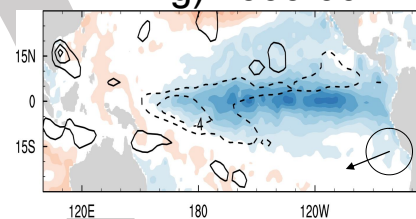
a) 1st EOF pattern (48.92%)



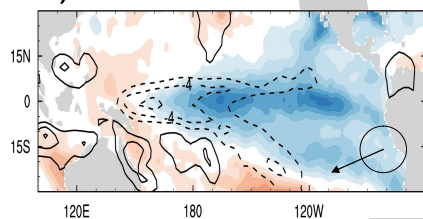
b) 2nd EOF pattern (10.43%)



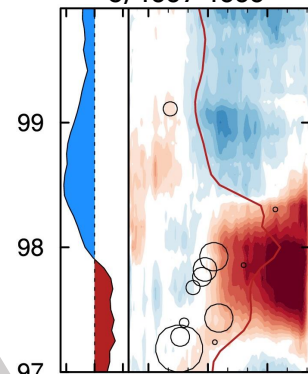
g) 1999/00 LN



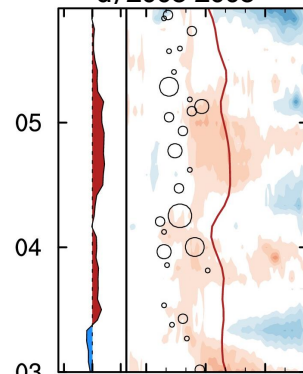
k) 2010/11 LN



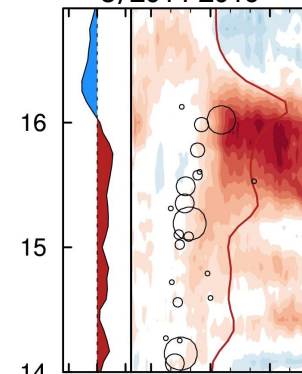
c) 1997-1999



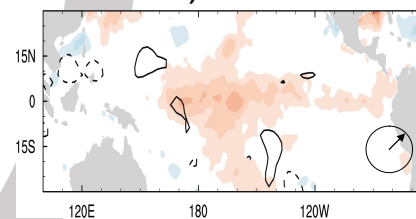
d) 2003-2005



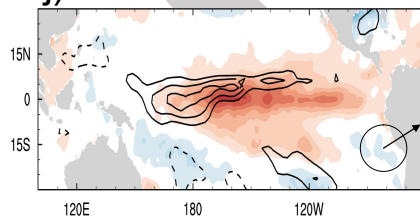
e) 2014-2016



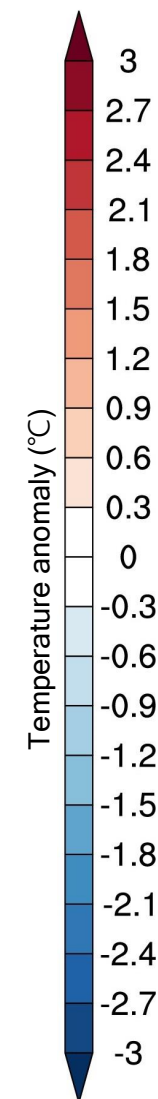
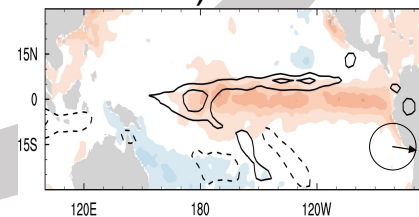
h) 2004/05 EN

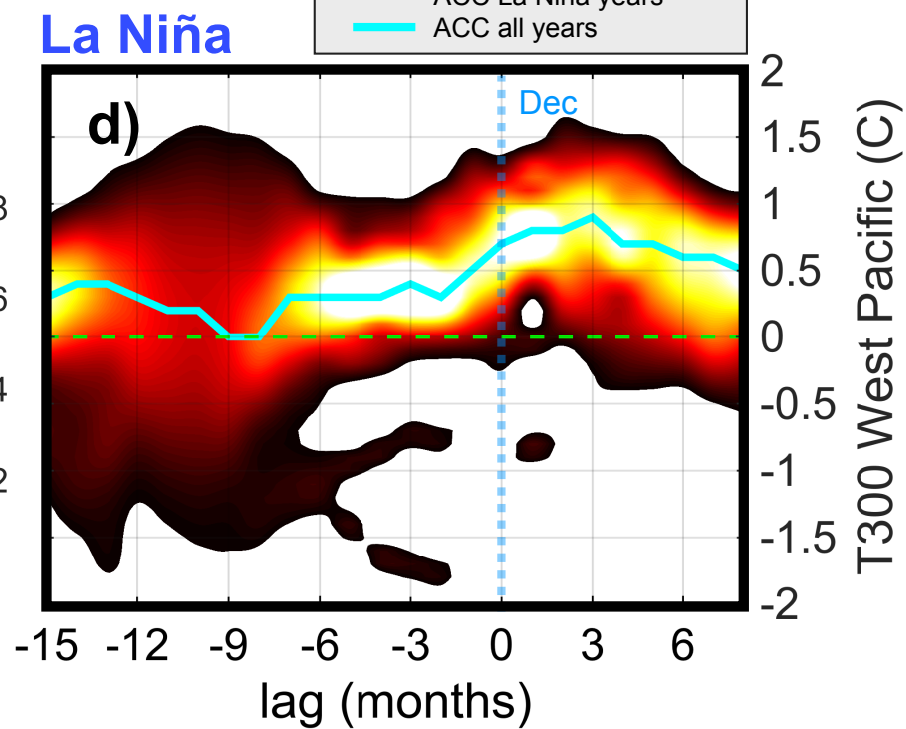
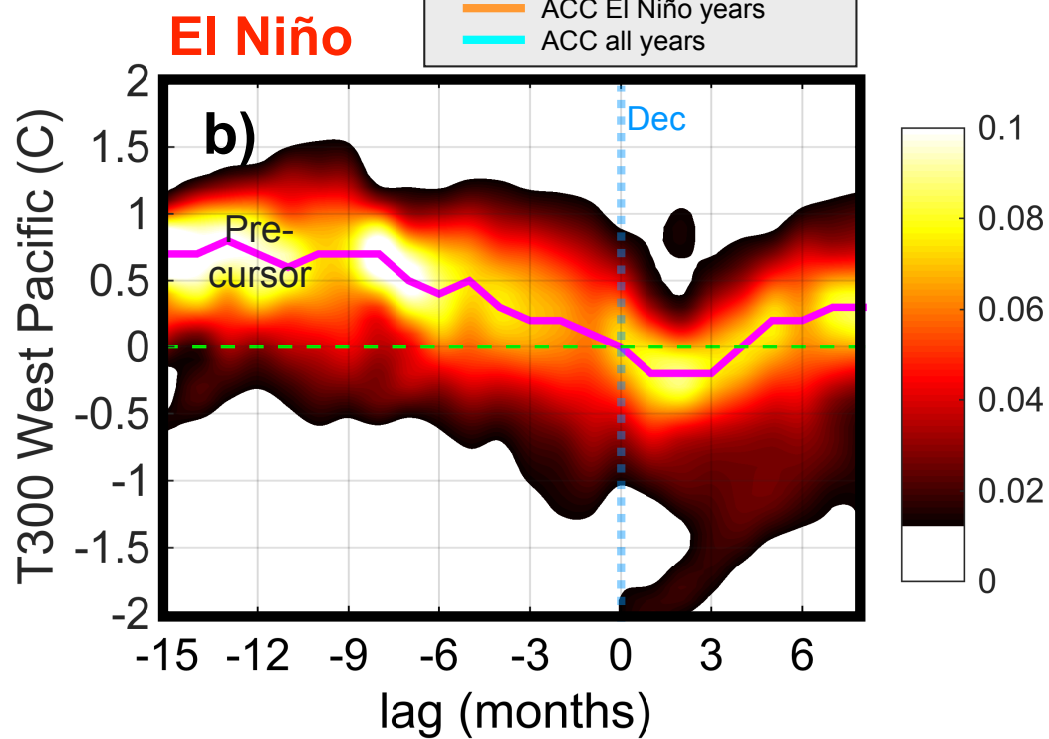
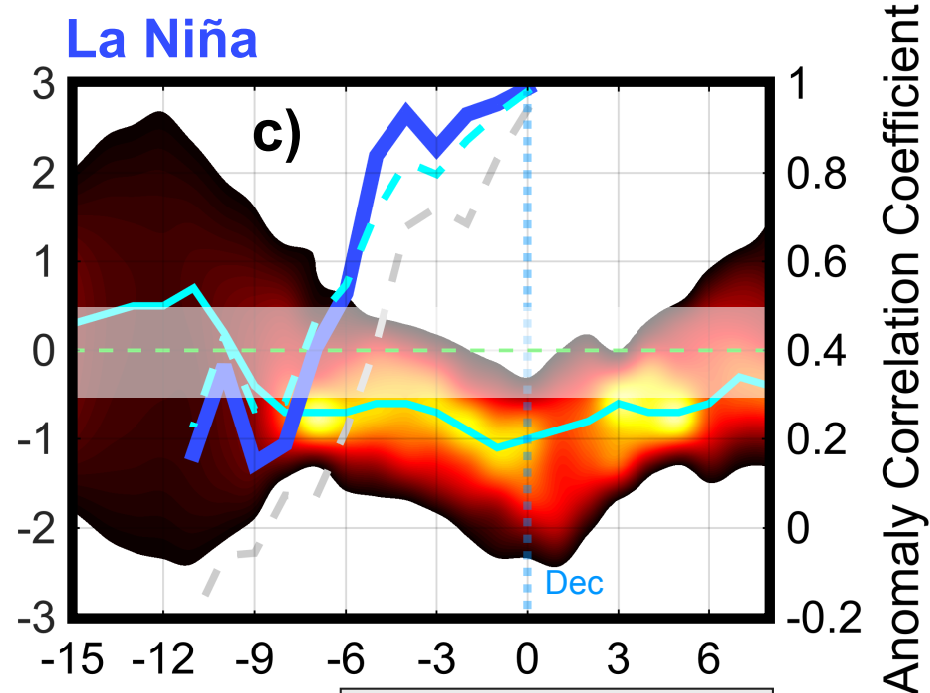
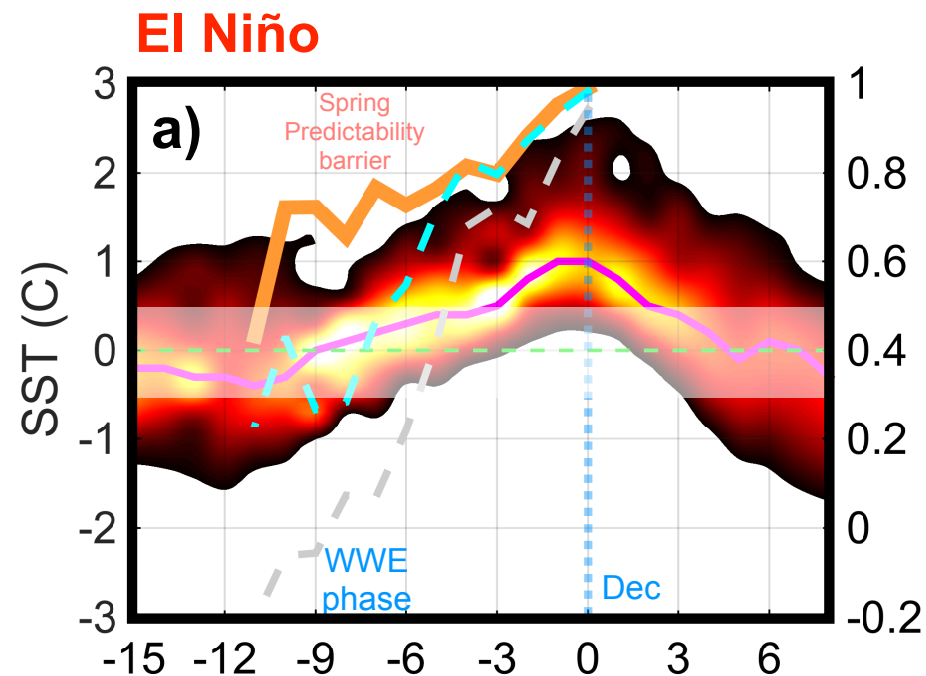


j) 2009/10 EN

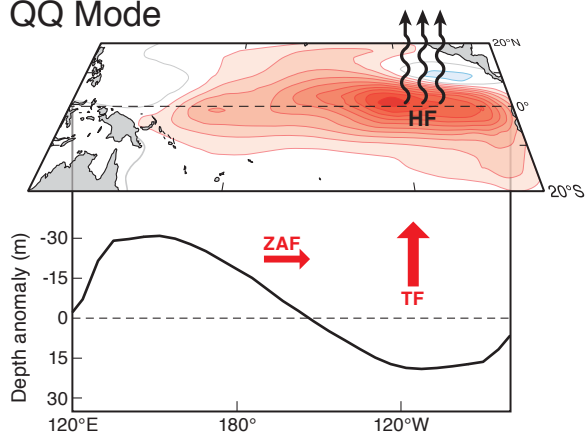


i) 2006/07 EN

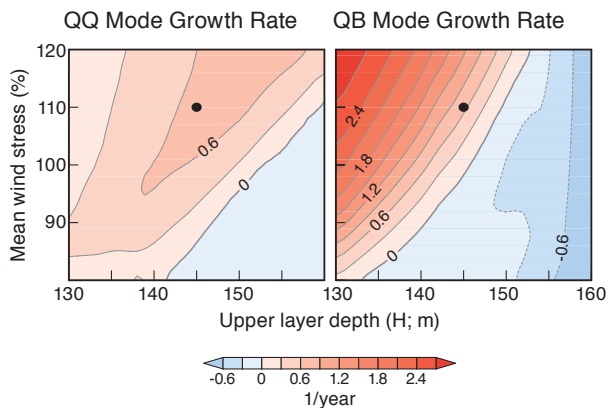
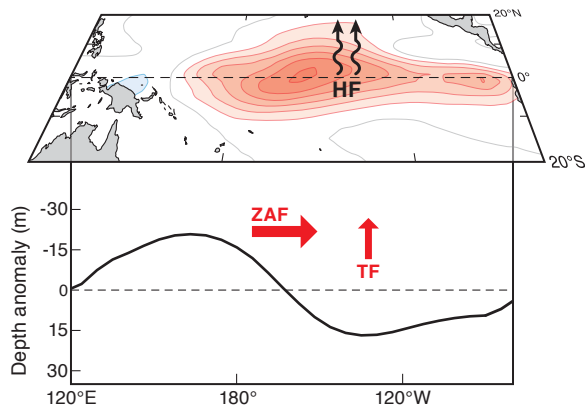




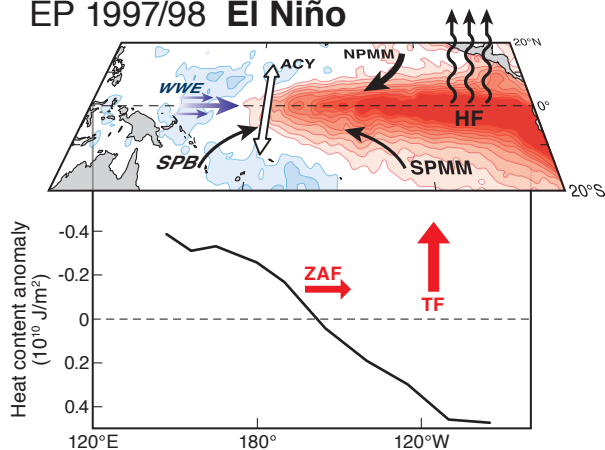
QQ Mode



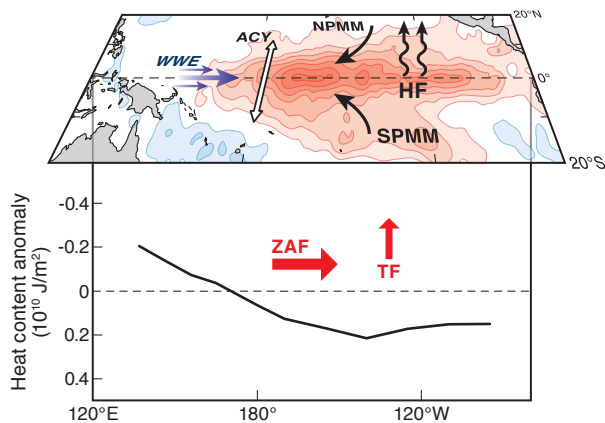
QB Mode



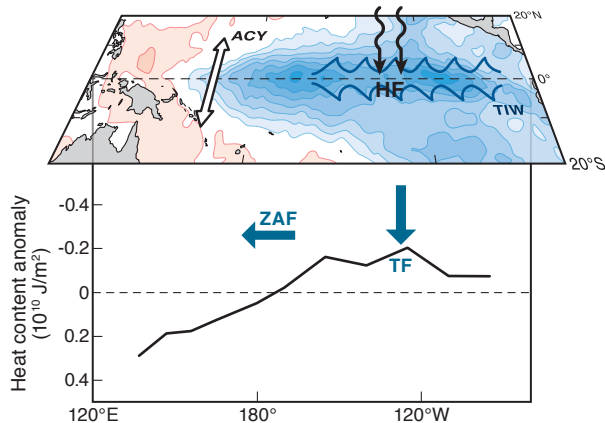
EP 1997/98 El Niño



CP 2009 El Niño



2010 La Niña



Indian Ocean, Atlantic Ocean, and other external forcings